VIII International Conference on Computational Methods for Coupled Problems in Science and Engineering
COUPLED PROBLEMS 2019
E. Oñate, M. Papadrakakis and B. Schrefler (Eds)

A METHOD FOR MULTI-OBJECTIVE TOPOLOGY OPTIMIZATION OF ACOUSTIC AND FLUID FLOW PROPERTIES

JAKOB MUNZ AND MICHAEL SCHÄFER

Institute of Numerical Methods in Mechanical Engineering
Technische Universität Darmstadt
Dolivostraße 15, 64293 Darmstadt, Germany
e-mail: munz@fnb.tu-darmstadt.de, web page: https://www.fnb.tu-darmstadt.de/

Key words: Coupled Problems, Brinkman Penalization, Impedance Mismatch, NURBS

Abstract. A framework for multi-objective topology optimization is presented with the purpose to simultaneously optimize both fluid flow and acoustic quantities. The proposed method uses a coupled approach on fixed grids with immersed solid boundaries. For the fluid flow part the incompressible Navier-Stokes equations are solved and the immersed boundaries are modeled with a Brinkman penalization method. The acoustic field is computed by an acoustic/viscous splitting technique and the solution of the resulting linearized Euler equations. The reflecting boundaries are modeled by a mismatch in the acoustic impedance between solid and fluid. To describe the geometry of the boundaries a NURBS-based approach is introduced. Two test cases are investigated to validate the immersed boundary method for the fluid flow problem and the acoustics, respectively. Finally, the capability for topological changes of the proposed method is shown with a multi-objective optimization test case, which is solved with the gradient-free evolutionary algorithm NSGA-II.

1 INTRODUCTION

Topology optimization is a commonly used method in various fields of engineering for improving the design of a product or individual components of it in an early stage of development. Used in the past mainly for structural optimization, it has recently gained increasing attention in other disciplines such as fluid flow or acoustic optimization. However, not much research has been done in simultaneously optimizing the acoustic as well as the fluid flow properties of a coupled problem in a multi-objective manner. This paper therefore deals with the topology optimization of such problems and presents a framework that can be used for this purpose.

Usually, non-body-fitted fixed grids are used for topology optimization to avoid the difficulties that can arise when regenerating a body-fitted grid due to large deformations

or topological changes of the computational domain. For fluid flow problems, one possible approach to realize this, which is also used in the present work, is the Brinkman penalization method [1]. Here arbitrarily complex solid bodies can be introduced into the flow domain, which are modeled as a porous medium with a permeability approaching zero. In order to also consider acoustics in terms of a sound reflection of these bodies, an impedance mismatch between fluid and solid is introduced. This approach is also used by the Impedance Mismatch Method, which was originally proposed by Chung and Morris [2] for steady mean flows and later applied for unsteady non-uniform flows by Cohen et al. [3]. For the numerical description of the interface between solid and fluid an approach proposed by Munz and Schäfer [4] is used, which utilizes non-uniform rational basis splines (NURBS) and uses the coordinates of the control points as design variables. The NURBS allow complex geometries to be described with a small number of design variables compared to other approaches, making it possible to use gradient-free global optimization techniques, such as genetic algorithms. For the numerical solution of the fluid flow as well as the acoustic problem the block-structured in-house solver FASTEST [5] is used. The incompressible Navier-Stokes equations are solved with a finite volume discretization. For the acoustic field an acoustic/viscous splitting technique [6, 7, 8] is used and the acoustic quantities are computed with the linearized Euler equations.

The objective of this work is to investigate the proposed framework with respect to numerical accuracy of the immersed boundary method and its suitability for topology optimization. Two test cases are examined to validate the presented method. For the first problem, a steady flow around a cylinder in a channel is investigated without considering the acoustics and the results are compared with results from the literature. In the second test case, the acoustic scattering of a Gaussian pulse from a cylinder is simulated and the results are compared with an analytical solution. Finally, the capability for topological changes of the proposed method is shown with a multi-objective optimization test case. Here the pressure drop of a channel flow and the acoustic permeability of the channel are minimized simultaneously. The gradient-free Non-dominated Sorting Genetic Algorithm II (NSGA-II) [9] is used to optimize these two competing objective functions.

2 NUMERICAL FRAMEWORK

In the following, the framework for topology optimization of multi-objective problems is presented. First the numerical description of the interface is discussed. Then the governing equations are introduced and a short overview of the optimization is given. Finally, the process of the complete framework is summarized.

2.1 Numerical description of the interface

The basis of the presented framework is a NURBS-based approach to describe the interface between solid and fluid, which was proposed by Munz and Schäfer [4]. Here the control point coordinates of the NURBS are coupled to the design variables of the

optimization algorithm, which allows the optimizer to change the geometry of the interface. The NURBS are, in the two-dimensional case, transformed into polygons, which are then used to calculate the volume fraction φ of the solid in each control volume. This leads to the three possible cases

$$x_i \in \begin{cases} \Omega_\mathrm{f} & \text{if } \varphi\left(x_i\right) = 0, \\ \Omega_\mathrm{s} & \text{if } \varphi\left(x_i\right) = 1, \\ \partial\Omega_\mathrm{s} & \text{if } 0 < \varphi\left(x_i\right) < 1, \end{cases} \tag{1}$$

where Ω_f is the fluid part of the computational domain, Ω_s is the solid part and $\partial\Omega_\mathrm{s}$ is the interface between the two. Here, a smooth transition at the interface is necessary to obtain a continuous objective function. The volume fraction is calculated using the Sutherland-Hodgman algorithm [10]. In this algorithm the polygons derived from the NURBS curves are clipped against each control volume. The area of the resulting clipped polygon is then set in ratio to the total area of the control volume to determine the volume fraction of the solid. By introducing multiple NURBS, which may overlap each other or disappear, it is also possible to realize topological changes in the domain during the optimization process. The disappearance is achieved by the fact that the algorithm for calculating the volume fraction is designed to return a negative value if a polygon or parts of a polygon "twist". This means that these parts of the polygon change their counting direction, for example from clockwise to counterclockwise. A negative volume fraction is then assumed to be equal to a volume fraction of zero.

2.2 Governing equations

For the derivation of the aeroacoustic equations an acoustic/viscous splitting technique is used, which was originally proposed by Hardin and Pope [6], then slightly modified by Shen and Sørensen [7] and later further developed by Kornhaas [8]. Here the fluid flow quantities are decomposed into an incompressible part and an acoustic perturbation, which reads

$$\rho = \rho^\mathrm{inc} + \rho^\mathrm{ac}, \qquad u_i = u_i^\mathrm{inc} + u_i^\mathrm{ac}, \qquad p = p^\mathrm{inc} + p^\mathrm{ac}, \tag{2}$$

with the density ρ, the flow velocity u_i and the pressure p. The superscript $(\,\cdot\,)^\mathrm{inc}$ indicates the incompressible part and the superscript $(\,\cdot\,)^\mathrm{ac}$ the acoustic perturbation.

Fluid flow equations To compute the fluid flow, the incompressible Navier-Stokes equations are solved. In order to take the immersed boundaries into account, the momentum equation is extended by a penalization term. The equations then read

$$\frac{\partial u_i^\mathrm{inc}}{\partial x_i} = 0, \tag{3}$$

$$\rho^\mathrm{inc}\frac{\partial u_i^\mathrm{inc}}{\partial t} + \rho^\mathrm{inc}\frac{\partial\left(u_i^\mathrm{inc}u_j^\mathrm{inc}\right)}{\partial x_j} = \frac{\partial}{\partial x_j}\left[\mu\left(\frac{\partial u_i^\mathrm{inc}}{\partial x_j} + \frac{\partial u_j^\mathrm{inc}}{\partial x_i}\right)\right] - \frac{\partial p^\mathrm{inc}}{\partial x_i} + \rho^\mathrm{inc}f_i - \alpha u_i^\mathrm{inc}, \tag{4}$$

with the time t, the dynamic viscosity μ, the external body forces f_i and the Brinkman penalization parameter

$$\alpha(\varphi) = \alpha_\mathrm{f} + (\alpha_\mathrm{s} - \alpha_\mathrm{f})\,\varphi, \tag{5}$$

where α_f refers to the fluid region and α_s to the solid region. The value for α_f is set to zero for the present work, which, together with the volume fraction φ, causes the penalization term to disappear in the fluid area, leading to the original Navier-Stokes equations. To realize the no-slip boundary condition at the interface of the solid, a high value for α_s has to be chosen, which causes the flow velocity in the solid to approach zero. According to [11], where a value of $\alpha > 10^4$ is suggested as sufficiently large, the value inside the solid parts is set to $\alpha_\mathrm{s} = 10^5$ for the present work.

Acoustic equations For the computation of the acoustics the linearized Euler equations

$$\frac{\partial \rho^\mathrm{ac}}{\partial t} + \rho^\mathrm{inc}\frac{\partial u_i^\mathrm{ac}}{\partial x_i} + u_i^\mathrm{inc}\frac{\partial \rho^\mathrm{ac}}{\partial x_i} = 0, \tag{6}$$

$$\rho^\mathrm{inc}\frac{\partial u_i^\mathrm{ac}}{\partial t} + \rho^\mathrm{inc}u_j^\mathrm{inc}\frac{\partial u_i^\mathrm{ac}}{\partial x_j} + \frac{\partial p^\mathrm{ac}}{\partial x_i} = 0, \tag{7}$$

$$\frac{\partial p^\mathrm{ac}}{\partial t} + c^2\rho^\mathrm{inc}\frac{\partial u_i^\mathrm{ac}}{\partial x_i} + u_i^\mathrm{inc}\frac{\partial p^\mathrm{ac}}{\partial x_i} = -\frac{\partial p^\mathrm{inc}}{\partial t} \tag{8}$$

are solved with the speed of sound c. To obtain the reflection of the acoustic waves at the immersed boundaries, the density ρ^inc is increased. This causes a mismatch in the acoustic impedance

$$Z = \rho^\mathrm{inc} c \tag{9}$$

between fluid and solid. According to the reflection coefficient

$$C_r = \frac{p_\mathrm{ref}}{p_\mathrm{in}} = \frac{Z_2 - Z_1}{Z_2 + Z_1} \tag{10}$$

this leads to a reflection of the sound wave. Here p_in is the incident and p_ref is the reflected acoustic pressure. The impedance of the fluid is Z_1 and the impedance of the solid is Z_2. For $Z_2 = Z_1$ the reflection coefficient equals zero and therefore no reflection occurs. For $Z_2 > Z_1$ the value of C_r becomes positive, so there is reflection without a phase change, which is the desired behaviour. On the other hand, for $Z_2 < Z_1$ the value of C_r becomes negative and thus the acoustic wave experiences a phase reversal. Therefore, the density is defined as

$$\rho^\mathrm{inc}(\varphi) = \rho_\mathrm{f}^\mathrm{inc} + \left(\rho_\mathrm{s}^\mathrm{inc} - \rho_\mathrm{f}^\mathrm{inc}\right)\varphi, \tag{11}$$

where $\rho_\mathrm{f}^\mathrm{inc}$ refers to the density in the fluid and $\rho_\mathrm{s}^\mathrm{inc}$ to density in the solid. In the present work the solid density is increased by a factor of 1000 compared to the fluid density. This leads to a theoretical amplitude error of the reflected wave of 0.2 % according to equation (10). It should be noted that the increased density is only used to compute the acoustics.

2.3 Optimization

The last part of the framework is the optimizer. There are a variety of optimization methods to perform a multi-objective optimization, which can be roughly divided into gradient-free and gradient-based methods. A gradient-based optimization can be advantageous in terms of computational speed, especially with a large number of design variables, if an adjoint method is used. However, one major problem with these methods is that they tend to get stuck in local minima, which can occur especially during topology optimizations, since the value of the objective function can change abruptly due to a change in the topology of the computational domain. To overcome this problem, the present work uses the comparatively small number of design variables resulting from the NURBS-based approach to make it feasible to use the gradient-free evolutionary algorithm NSGA-II.

2.4 Procedure of the framework

The complete process of a multi-objective topology optimization with the presented framework is shown schematically in Figure 1 and can be summarized as follows:

1. Generation of NURBS depending on design variables
2. Derivation of polygons $\mathbf{P}$ and transfer to the fluid flow as well as to the acoustic solver
3. Calculation of volume fractions using the Sutherland-Hodgman algorithm within the solver
4. Solving flow equations and transfer of fluid objective function $\mathcal{J}^{\mathrm{f}}$ to the optimizer as well as transfer of resulting fluid flow quantities to the acoustic solver
5. Solving acoustic equations and transfer of acoustic objective function $\mathcal{J}^{\mathrm{a}}$ to the optimizer
6. Checking convergence criteria and repeating the process if criteria are not reached

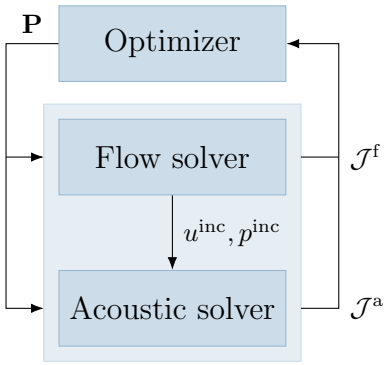

Figure 1: Procedure of a multi-objective topology optimization

3 VALIDATION

To validate the proposed method, two different test cases are investigated. First a steady channel flow around a cylinder at $\mathrm{Re} = 20$ is simulated. The cylinder is modeled with the Brinkman penalization method and the results are compared to results from literature. For the second test case, the acoustic scattering of a Gaussian pulse from a cylinder is simulated. To model the reflecting solid boundaries, a mismatch in the acoustic impedance between fluid and solid is introduced. The acoustic pressure is measured over time at three monitoring points and the results are compared with an analytical solution.

3.1 Steady channel flow around a cylinder

The first test case is intended to investigate the suitability of the Brinkman penalization method for modeling solid boundaries. For this purpose, a two-dimensional steady flow around a circular cylinder in a channel is considered. The benchmark problem is taken from [12], where it is referred to as test case 2D-1 and where several results for different solution approaches can be found. The geometry of this test case is shown in Figure 2. The kinematic viscosity is set to $\nu = 0.001\,\mathrm{m^2\,s^{-1}}$ and the fluid density to $\rho = 1.0\,\mathrm{kg\,m^{-3}}$.

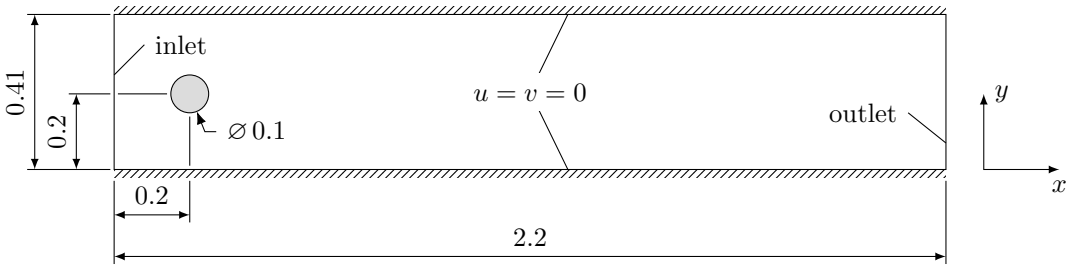

Figure 2: Geometry and boundary conditions of the channel flow test case

At the inlet, a parabolic flow velocity profile

$$u\,(0, y) = 4u_m y \left(\frac{h - y}{h^2}\right), \quad v = 0 \tag{12}$$

is applied with the channel height $h = 0.41\,\mathrm{m}$ and the maximum flow velocity $u_m = 0.3\,\mathrm{m\,s^{-1}}$, which leads to a Reynolds number of $\mathrm{Re} = \bar{u}d/\nu = 20$. Here the mean velocity is defined as $\bar{u} = 2u_m/3$. The Brinkman penalization parameter is set to $\alpha = 10^5$. The results of the simulations are compared with two of the criteria that can be found in [12]. These are the length of the recirculation zone L_a, as well as the pressure difference between the front and the back of the cylinder ΔP. The computations are carried out on three successively refined grids with a maximum of 800×400 control volumes. The values of the volume fraction in the vicinity of the cylinder are shown exemplary for the coarsest grid in Figure 3 and the results of the simulations are shown in Table 1. For both criteria, the results are

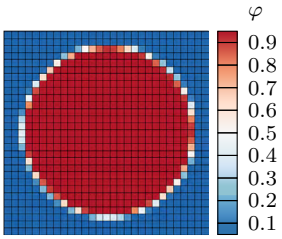

Figure 3: Volume fraction

Grid	L_a	ΔP
200×100	0.0847	0.1185
400×200	0.0844	0.1167
800×400	0.0849	0.1175
2D-1 [12]	$[0.0842, 0.0852]$	$[0.1172, 0.1176]$

Table 1: Benchmark results

in the range of the results of [12]. Therefore, it is assumed that the Brinkman penalization method is suitable to model solid boundary conditions.

3.2 Scattering of acoustic waves from a cylinder

The second benchmark test case is an acoustic two-dimensional initial value problem without background flow. It is particularly well suited to investigate the scattering of acoustic waves at curved solid boundaries as they can usually occur during topology optimization. The test case corresponds to problem 2 of category 2 in [13], where an analytical solution to this problem can also be found. All variabes are non-dimensionalized using the diameter d of the cylinder as length scale, c as velocity scale, d/c as time scale, $\rho_\mathrm{f}^\mathrm{inc}$ as density scale and $\rho_\mathrm{f}^\mathrm{inc}c^2$ as pressure scale. The basic configuration of the test case is shown in Figure 4. Here, the circular cylinder is located in the center of a square

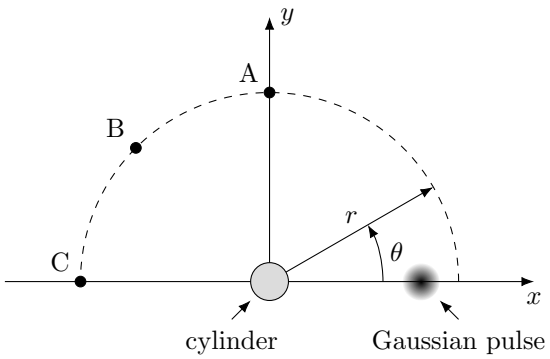

Figure 4: Schematic diagram of the acoustic scattering test case

computational domain with $x, y \in [-10, 10]$. Next to this cylinder a Gaussian pressure wave is initiated. This pressure wave then propagates over time, is reflected from the cylinder and finally leaves the computational domain. The acoustic pressure is measured over time at the three monitoring points A ($r = 5$, $\theta = 90°$), B ($r = 5$, $\theta = 135°$) and C ($r = 5$, $\theta = 180°$). Since there is only an interest to investigate whether the introduced impedance mismatch is suitable to model solid boundaries, the half-width of the Gaussian pulse is increased compared to the original test case in order to reduce the influence of numerical diffusion. The density of the solid is set to $\rho_\mathrm{s}^\mathrm{inc} = 1000$ and the center of the Gaussian pulse is located at $x_s = 4$ and $y_s = 0$ with the half-width $w = 0.5$. The initial conditions for this test case are $t = 0$, $u^\mathrm{ac} = v^\mathrm{ac} = 0$ and

$$p^\mathrm{ac} = \exp\left[-\ln 2\left(\frac{(x-x_s)^2 + (y-y_s)^2}{w^2}\right)\right]. \tag{13}$$

The problem is solved on three successively refined Cartesian grids with 512×512, 1024×1024 and 2048×2048 control volumes. To avoid spurious oscillations the Osher

flux limiter [14] with $\beta = 1$ is used according to [8]. The time step size is $\Delta t = 0.0125$ for the coarsest, $\Delta t = 0.00625$ for the medium and $\Delta t = 0.003125$ for the finest grid, yielding a constant acoustic CFL number of 0.32. Figure 5 shows the contour plots of the acoustic pressure for the time steps $t = 2, 4, 6$ on the finest grid. As can be seen,

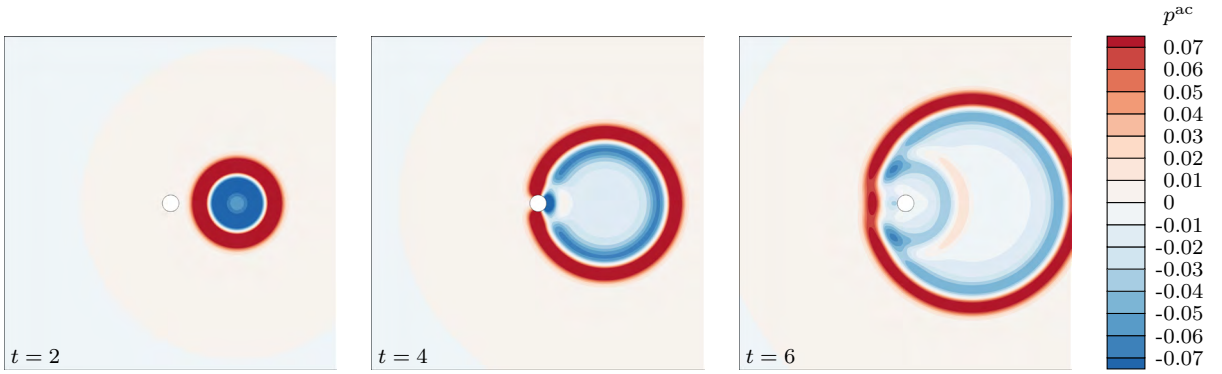

Figure 5: Scattering of the initial Gaussian pulse from the cylinder at different time steps

the acoustic wave propagates smoothly in the computational domain and is scattered at the cylinder. Figure 6 compares the results of the simulations with an analytical solution for the three monitoring points in the time interval from $t = 5$ to $t = 11$. For

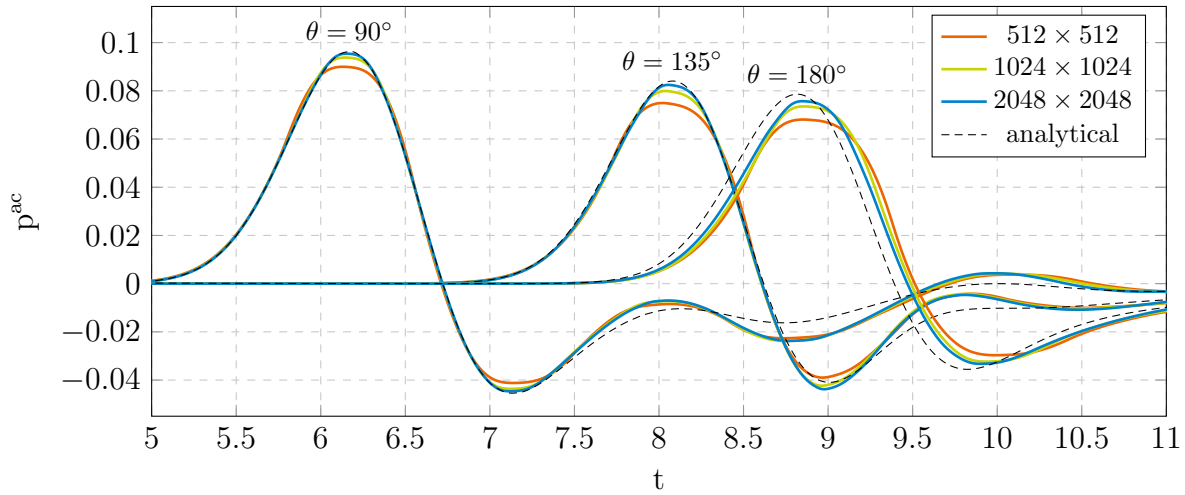

Figure 6: Acoustic pressure over time for the scattering of the Gaussian pulse at the three monitoring points

the undisturbed acoustic wave, which first reaches point A ($\theta = 90°$) and then point B ($\theta = 135°$), the amplitude approaches the analytical solution as the grid size increases. At point C ($\theta = 180°$), however, the wave diffracted by the cylinder shows a time-shift

of about $\Delta t = 0.01$ compared to the analytical solution. In the further course, the wave scattered from the cylinder reaches the monitoring points where it shows an amplitude error which is almost independent of the grid size. Nevertheless, the main characteristics of the wave propagation are correctly represented and the simulation is generally in good agreement with the analytical solution. In addition, topology optimization is essentially about creating a first draft rather than a detailed design, so the accuracy achieved is sufficient to use the proposed approach for topology optimization.

4 APPLICATION TO MULTI-OBJECTIVE OPTIMIZATION

In the following, a multi-objective topology optimization of a two-dimensional channel is investigated. Two competing objective functions are considered, which are the pressure drop between inlet and outlet as well as the acoustic permeability of the channel, both of which should be minimized. The geometry of the test case is shown in Figure 7. In

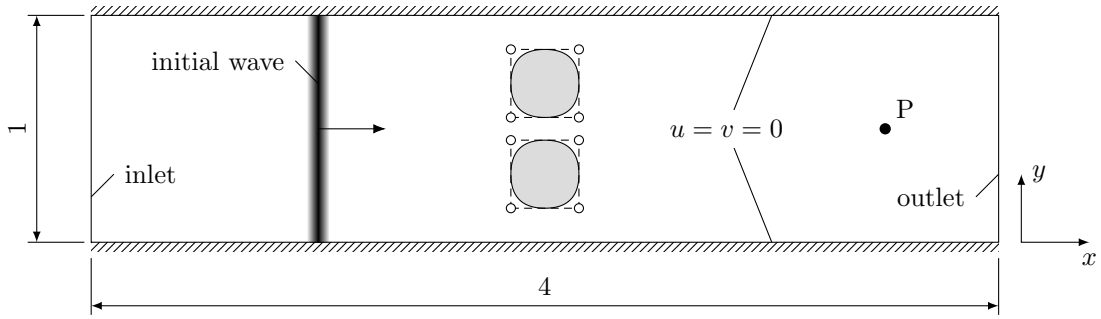

Figure 7: Geometry of the two-dimensional optimization test case

order to quantify the acoustic permeability, an acoustic wave is initiated at the position $x_s = 1.0\,\mathrm{m}$ with the initial conditions

$$p^{\mathrm{ac}} = 1.5 \exp\left[-\ln 2 \left(\frac{(x - x_s)^2}{w^2}\right)\right] \mathrm{N\,m^{-2}}, \tag{14}$$

$$u^{\mathrm{ac}} = 0.001 \exp\left[-\ln 2 \left(\frac{(x - x_s)^2}{w^2}\right)\right] \mathrm{m\,s^{-1}}, \quad v^{\mathrm{ac}} = 0\,\mathrm{m\,s^{-1}}, \tag{15}$$

and a half-width of $w = 0.05\,\mathrm{m}$. The speed of sound is set to $c = 1000\,\mathrm{m\,s^{-1}}$. Two closed NURBS curves, whose shapes are varied by the optimization, are introduced into the channel. Both of these curves are defined by six control points, whereby the first two points are repeated according to the degree of the curves. The positions of the control points are defined relative to the centers of the curves, which are $(2.0, 0.3)$ and $(2.0, 0.7)$. An unclamped, uniform node vector $U = \{0, \ldots, 8\}$ is used and all weights are set to one. Each of the control point coordinates is determined by a separate design variable, resulting in a total of 16 design variables. The upper and lower bounds of the design variables are defined

in such a way that there will always be a gap at the top and bottom of the channel, but the curves can overlap in the middle. The acoustic pressure is measured at the monitoring point P = (3.5, 0.5) and the maximum value within a time interval of $\Delta t = 0.004\,\mathrm{s}$ is determined and used as objective function. For the inlet boundary condition, a parabolic flow velocity profile according to equation (12) is used with a channel height $h = 1\,\mathrm{m}$ and a mean flow velocity $\bar{u} = 20\,\mathrm{m\,s^{-1}}$. The kinematic viscosity is set to $\nu = 1.0\,\mathrm{m^2\,s^{-1}}$ and the fluid density to $\rho_\mathrm{f}^\mathrm{inc} = 1.0\,\mathrm{kg\,m^{-3}}$, which leads to a Reynolds number of Re = 20, based on the channel height. In order to obtain the sound reflection by the impedance mismatch, the solid density is set to $\rho_\mathrm{s}^\mathrm{inc} = 1000\,\mathrm{kg\,m^{-3}}$. Since two competing objective functions are to be optimized, the gradient-free NSGA-II is used. The two objective functions should then come into conflict, since it is expected that minimizing the pressure drop leads to a channel without obstacles, while the optimum for minimum acoustic permeability should correspond to the opposite, i.e. a channel with the largest possible reflective obstacles. The results of the topology optimization are shown in Figure 8 and as expected a set of Pareto optimal solutions can be seen. On the right side of Figure 8, the optimized

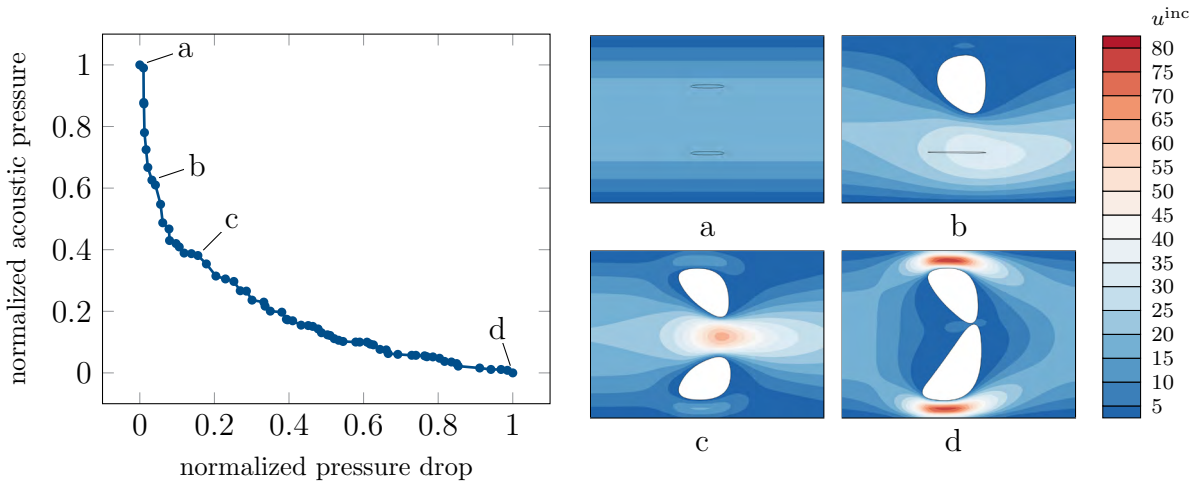

Figure 8: Pareto set of the multi-objective optimization and the geometry of four selected points (a-d) with the resulting flow velocity fields

geometries for the extreme points as well as for two other characteristic points from the Pareto front are shown as examples. In case of a minimal pressure drop (point a), the impermeable areas disappear as predicted because the polygons have twisted, as explained in section 2.1. On the way to a minimum of the acoustic permeability (point b and c), the two NURBS curves increasingly close the channel. At the optimum of the acoustic permeability (point d), the upper curve reaches the maximum height and the lower curve its minimum height. In the middle, however, the expected overlap does not occur, leaving a small gap between the two curves. At this point, the two curves approach each other until they both intersect the same control volume but do not cover it completely, resulting

in an intermediate value for the Brinkman penalization parameter and the impedance mismatch, respectively. This value is just large enough to reflect most of the incident acoustic wave, but not large enough to completely prevent the fluid flow between the two curves. This can also be seen in Figure 8 in the plot for point d, where the light blue area between the two curves indicates a slow but non-zero flow. The acoustic permeability has thus reached an optimum which additionally allows to reduce the pressure drop slightly compared to two overlapping curves. This state is actually not desired, since it is based on the unphysical assumption that there may be areas which are partially permeable. However, these intermediate values in the control volumes serve only to ensure smooth objective functions and should not to be exploited by the optimizer to improve an objective function. Further research is therefore needed at this point to prevent this behaviour.

5 CONCLUSIONS

A framework for multi-objective topology optimization of fluid flows and acoustics has been presented, which uses a coupled aeroacoustic solver for all computations. It is based on the solution of the incompressible Navier-Stokes equations for the fluid flow problem and an acoustic/viscous splitting technique together with the linearized Euler equations for the acoustic problem. For the fluid flow computations it uses the Brinkman penalization method to account for solid areas in the flow domain, while for the acoustics an impedance mismatch between solid and fluid is introduced. In both cases the geometry of the solid boundaries is mathematically described by NURBS curves. The control point coordinates of these NURBS are used as design variables, which has the advantage that complex geometries can be described with a relatively small number of parameters. Thus, the number of design variables can be reduced to such an extent that it is possible to use gradient-free optimization methods, like the Non-dominated Sorting Genetic Algorithm (NSGA-II).

The proposed method has been validated with two test cases taken from literature and has shown a good agreement. Finally, a multi-objective optimization problem has been investigated, which has basically shown the expected results, but also revealed a problem. The optimizer exploits the possible intermediate values in the control volumes to improve the objective functions. Although this is a logical result for the optimization, it was not expected and further research is needed to prevent such loopholes for the optimizer. The next step will be to use this coupled framework for the topology optimization of aeroacoustic problems, where the acoustic sources are generated by the fluid flow.

REFERENCES

[1] Angot, P., Bruneau, C.-H. and Fabrie, P. A penalization method to take into account obstacles in incompressible viscous flows. *Numer. Math.* (1999) **81**(4):497–520.

[2] Chung, C. and Morris, P.J. Acoustic scattering from two-and three-dimensional bodies. *J. Comput. Acoust.* (1998) **6**(3):357–375.

[3] Cohen, R., Ooi, A. and Iaccarino, G. Towards the application of the impedance mismatch method to the expansion about incompressible flow acoustic equations. *Proc. Summer Program 2006, Center for Turbulence Research* (2006) 559–571.

[4] Munz, J. and Schäfer, M. A NURBS-based approach for shape and topology optimization of flow domains. *Proc. 6th ECCM, 7th ECFD* (2019) 3248–3257.

[5] Durst, F. and Schäfer, M. A Parallel Block-Structured Multigrid Method for the Prediction of Incompressible Flows. *Int. J. Numer. Methods Fluids* (1996) **22**(6):549–565.

[6] Hardin, J.C. and Pope, D.S. An acoustic/viscous splitting technique for computational aeroacoustics. *Theor. Comp. Fluid Dyn.* (1994) **6**(5-6):323–340.

[7] Shen, W.Z. and Sørensen, J.N. Comment on the aeroacoustic formulation of Hardin and Pope. *AIAA Journal* (1999) **37**(1):141–143.

[8] Kornhaas, M. Effiziente numerische Methoden für die Simulation aeroakustischer Probleme mit kleinen Machzahlen. *Ph.D. Thesis, Technische Universität Darmstadt* (2012).

[9] Deb, K., Pratap, A., Agarwal, S. and Meyarivan, T. A fast and elitist multiobjective genetic algorithm: NSGA-II. *IEEE transactions on evolutionary computation* (2002) **6**(2):182–197.

[10] Sutherland, I.E. and Hodgman, G.W. Reentrant polygon clipping. *Communications of the ACM* (1974) **17**(1):32-42.

[11] Kreissl, S., Pingen, G. and Maute, K. Topology optimization for unsteady flow. *Int. J. Numer. Methods Eng.* (2011) **87**(13):1229–1253.

[12] Schäfer, M., Turek, S., Durst, F., Krause, E. and Rannacher, R. Benchmark computations of laminar flow around a cylinder. *Flow simulation with high-performance computers II* (1994) 547–566.

[13] Tam, C. K. and Hardin, J.C. Second computational aeroacoustics (CAA) workshop on benchmark problems. *NASA Conference Publication 3352* (1997).

[14] Chakravarthy, S. and Osher, S. High resolution applications of the Osher upwind scheme for the Euler equations. *6th CFD Conference Danvers* (1983) 363–372.